RSC Applied Polymers

PAPER

View Article Online
View Journal | View Issue

Cite this: *RSC Appl. Polym.*, 2025, **3**, 1585

Sustainable and efficient preparation of eugenol-based resin and its application in UV-thermally cured 3D printing

Jieyuan Zheng,†[a,b] Xingfen Huang,†[a,b] Pingwei Liu,[a,b] Wenjun Wang *[a,b] and Hong Fan *[b,c]

Received 3rd June 2025,
Accepted 13th September 2025

DOI: 10.1039/d5lp00162e

rsc.li/rscapplpolym

To meet sustainable development demands, reducing non-renewable resource consumption while promoting material recycling has become imperative. For thermosetting resins, the commercialization of high-performance bio-based alternatives remains challenging due to biomass cost constraints and processing limitations. Herein, we demonstrate a facile method for large-scale preparation of a eugenol-derived thermoset monomer (EUEP) characterized by high yield, high purity, and low waste generation. Through acrylation modification, a fully bio-based resin system with dual UV-thermal curing capability was developed. The material's initial shape stabilization was rapidly achieved *via* UV-initiated radical polymerization, while subsequent thermally induced transesterification allowed precise modulation of covalent crosslinking network density. This sequential curing approach enabled controllable tuning of the resin's mechanical properties, achieving tensile strength ranging from 2 to 23 MPa with the corresponding elongation at break varying between 5% and 18%. Leveraging dynamic ester bond exchange at interfaces, the thermoset exhibited intrinsic crack-repairing and self-adhesion functionalities. This methodology establishes a novel strategy for developing fully bio-based reworkable resin systems, demonstrating significant potential for enhancing 3D printing process efficiency.

1 Introduction

Photopolymers are widely employed in electronics manufacturing, additive fabrication (3D printing), and dental applications owing to their notable advantages: rapid curing kinetics, energy-efficient processing, low capital investment requirements, and diminished volatile organic compound (VOC) emissions.[1–4] Nevertheless, heightened environmental awareness coupled with diminishing fossil fuel reserves has driven substantial research efforts toward sustainable material development using renewable resources.[5,6] A critical limitation arises from their stable permanent crosslinked networks, which impede recycling processes and prevent facile thermal repair of damaged/discarded materials, ultimately leading to significant environmental contamination.[7]

Dynamic covalent bonds (DCBs) have emerged as a promising strategy for designing recyclable thermosetting polymers, particularly in photopolymer systems.[8,9] These bonds undergo reversible cleavage and reformation under external stimuli such as thermal, photonic, or chemical activation,[10–12] enabling topological reorganization of polymer networks. This unique behavior effectively converts conventional thermosets into materials exhibiting thermoplastic-like processability. Various DCBs have been explored for recycling thermosets, such as ester,[13] imine,[14] Diels–Alder (DA),[15] disulfide,[16] and boronic ester DCBs.[17] Notably, DCBs can maintain network connectivity while exhibiting Arrhenius-like flow behavior during exchange reactions, a characteristic that defines them as "vitrimers".[18]

Within photopolymer systems, acrylate-based resins constitute a dominant commercial technology in both ink formulations and additive manufacturing, primarily owing to their rapid processing kinetics and adjustable mechanical performance. The ester functionalities within these polymers serve as critical sites for dynamic covalent reorganization, enabling the transformation of thermosetting photopolymers into vitrimeric materials. Zinc(II) salts, particularly zinc acetate ($Zn(OAc)_2$), have been widely adopted as effective transesterification catalysts. Seminal work by Leibler's group[19] established concentration-dependent control of exchange kinetics in ester-based networks through $Zn(OAc)_2$ modulation. Subsequent

[a]*Institute of Zhejiang University – Quzhou, 99 Zheda Road, Quzhou 324000, China*
[b]*College of Chemical and Biological Engineering, Zhejiang University, Hangzhou 310027, China. E-mail: hfan@zju.edu*
[c]*Wenzhou Advanced Materials International Sci-Tech Innovation Center, Institute of Wenzhou, Zhejiang University, Wenzhou 325006, China*
†These authors contributed equally.

studies by Tournilhac *et al.*[20] revealed that Zn^{2+} coordination with ester groups enhances carbonyl electrophilicity while stabilizing nucleophilic alkoxide intermediates. Zhang and coworkers[21] pioneered the development of $Zn(acac)_2$-catalyzed photopolymers with 3D-printable, self-healing capabilities *via* intercatenary transesterification. This dynamic bonding mechanism not only increased network crosslink density but also enhanced cured resin tensile strength by 40% relative to conventional systems. Nevertheless, absolute tensile strengths remain constrained (15 MPa), while persistent dependence on petrochemical monomers continues to hinder sustainable implementation.

Bio-based feedstocks are emerging as pivotal components in sustainable material innovation, motivated by escalating ecological imperatives and finite petroleum reserves. Substantial research progress has been documented for biomass-derived precursors including lignin,[22] vanillin,[23] eugenol,[24] vegetable oils,[25] and furan compounds,[26] with varying technology readiness levels. While triglyceride derivatives and cardanol-based systems have achieved industrial adoption, their cured networks frequently display compromised mechanical integrity due to structural limitations inherent in their long aliphatic chains. Conversely, rigid bio-based monomers such as eugenol, vanillin derivatives, and furan-based architectures have demonstrated superior performance metrics to petroleum-based analogs like bisphenol A-glycidyl methacrylate (BisGMA) in terms of modulus and thermal stability.[27–29] Eugenol, a naturally occurring phenolic compound from clove oil, has attracted significant interest as a thermoset precursor owing to its multiple reactive sites (allyl, aromatic, and phenolic hydroxyl groups) and cost-effectiveness. Our team recently developed a novel synthesis protocol for high-purity eugenol epoxy (EUEP) under solvent-free conditions, demonstrating exceptional performance in UV-curable coating formulations.[30,31] Despite these advancements, eugenol-based photopolymer development remains predominantly confined to laboratory-scale investigations, with persistent obstacles in scalable production and unresolved processing complexities hindering industrial implementation.

In this study, we report for the first time a scalable and green synthesis process for a bio-based aromatic epoxy resin. A method was developed for the synthesis of a high-purity eugenol-based epoxy monomer (EUEP), which also enables the efficient recycling of raw materials. Subsequently, a resin monomer capable of UV-thermal dual curing was developed through the acrylation of EUEP. The resin is first cured by UV radiation *via* its unsaturated double bonds to establish the material's basic shape. During the subsequent thermal curing stage, dynamic transesterification reactions involving the abundant ester and hydroxyl groups are utilized to modulate the cross-linking density, thereby tuning the resin's mechanical properties. Furthermore, the presence of these dynamic ester bonds endows the material with reparability and reprocessability. This has been applied in 3D printing, where the material demonstrates unique welding capabilities.

2 Experiments

2.1 Materials

Eugenol (99%), epichlorohydrin (ECH, 99%), benzyl triethyl ammonium chloride (TEBA, 98%), Karstedt catalyst (2 wt% platinum in xylene), and NaOH (>98%) were supplied by Shanghai Aladdin Biochemical Technology Co., Ltd. 1,1,3,3-Tetramethyl disiloxane (HMM, 99%) and hexamethyldisiloxane (MM, 99%) were provided by United Chemicals. Tetraethyl orthosilicate (TEOS, 99%), ethanol (AR), toluene (AR), acrylic acid (AR, >99%), and HCl (37% aqueous solution) were obtained from Sinopharm Chemical Reagent Co., Ltd. *p*-Methoxyphenol (99%) and $Zn(acac)_2$ (99%) were supplied by Macklin. Phenylbis(2,4,6-trimethylbenzoyl) phosphine oxide (≥97%) was provided by Shanghai Xianding Biotechnology Co., Ltd as the photoinitiator.

2.2 Characterization

The GC-MS analysis was performed utilizing Agilent 6890/5973 apparatus using a ZB-5MS column with dimensions of 30 m × 0.25 mm × 0.5 μm, with H_2 as the carrier gas. The GC heating program is detailed below: the inlet was set to 270 °C, and the column was initially held at 80 °C for two minutes. Following this, the temperature was ramped at 20 °C min^{-1} until 250 °C was reached, which was then maintained for 10 minutes to ensure complete sample vaporization. The detector temperature was adjusted to 300 °C, while the MS was run with an electron energy of 70 eV. Nuclear magnetic resonance (NMR) spectra were recorded on a Bruker Avance DRX 500 using chloroform-d as the solvent under ambient conditions. The Fourier transform infrared (FT-IR) spectra were obtained using a Nicolet 5700 spectrometer. ATR techniques and potassium bromide pellets were both used, with the wavenumber range spanning 400 to 4000 cm^{-1}. The thermal decomposition of the cured samples was studied with a thermogravimetric analyzer (Q500, TA instruments) under a nitrogen atmosphere (40 mL min^{-1}). The samples (~5 mg) were heated from 25 to 700 °C at 10 °C min^{-1}. A ZwickRoell Z020 was used to investigate the tensile properties of eugenol-based resins at a testing rate of 1.0 mm min^{-1}, following the guidelines of GB/T 1040.1-2018. For dynamic mechanical analysis (DMA), a TA Q800 instrument in dual cantilever mode was used, with a temperature range of −30 to 100 °C, a heating rate of 3 °C min^{-1}, and a frequency of 1 Hz. The sample dimensions were 15 mm × 5 mm × 1 mm. Stress relaxation studies were conducted using a HAKKE RS6000 rheometer, with the sample disk being 1 mm thick and 25 mm in diameter. After allowing the sample to reach equilibrium between the two plates of the instrument at a predetermined temperature for five minutes, a 1% strain was used. The time-dependent storage modulus was then recorded for analysis. A CREALITY LCD 3D printer was used to print the resin onto 3D objects; the printing was performed with a *z*-axis layer height of 50 μm and an individual layer exposure time of 10 s for an optimum printing quality.

2.3 The large-scale synthesis of EUEP

As outlined in Fig. 1a, the synthesis commenced with charging eugenol (25 kg, 152.44 mol), epichlorohydrin (ECH, 70 kg, 756.59 mol), and benzyltriethylammonium chloride (0.6 kg, 2.63 mol) into a jacketed reactor under a nitrogen atmosphere. The reaction mixture was maintained at 80 °C with vigorous agitation for 2 h to complete the etherification process. Following this, residual ECH was reclaimed through vacuum distillation (65 °C, 10 kPa). The system was subsequently cooled to 60 °C, whereupon an aqueous sodium hydroxide solution (24.4 kg, 50 wt%) was introduced *via* controlled addition over 30 min. After 3 h of continued reaction, phase separation yielded an organic layer containing crude EUEP, which was further purified to obtain a pale yellow viscous liquid and it crystallized at room temperature (yield: 91%, purity >98% by HPLC).

2.4 Synthesis of eugenol acrylate (EUAC)

EUEP (50 g, 0.23 mol) was transferred into a 250 mL flask which was three-necked for equipping the mechanical agitator and reflux condenser. A mixture of triphenylphosphine (0.8 g, 0.003 mol), acrylic acid (17 g, 0.24 mol), and *p*-methoxyphenol (0.67 g, 5 mmol) was prepared and added into the flask dropwise over half an hour. The resulting solution was vigorously agitated at 100 °C until the acid value dropped below 5 mg KOH per g. After cooling to room temperature, the light-yellow, transparent liquid EUAC was obtained.

^{1}H-NMR: 6.83 (d, 1H, ArH), 6.71 (m, 2H, ArH), 6.40 (m, 1H, CH), 6.13 (m, 1H, CH), 5.91 (m, 1H, CH), 5.79 (m, 1H, CH), 5.06 (m, 2H, CH_2), 4.54 (m, 1H, CH), 4.29 (m, H, CH_2), 4.10–3.94 (m, 4H, CH_2), 3.78 (s, 3H, CH_3), 3.31 (m, 2H, CH_2).

2.5 Synthesis of eugenol acrylate MQ silicone resin (EUAC-MQ)

A mixture of MM (7.28 g, 0.04 mol), HMM (12 g, 0.09 mol), EtOH (9 g, 0.2 mol), H_2O (15 g, 0.83 mol), and 37% aqueous HCl solution (2.2 g, 0.02 mol) was added into a glass flask fitted with a reflux condenser. The mixture was slowly heated to 70 °C, at which point TEOS (40 g, 0.2 mol) was introduced dropwise, allowing the reaction to proceed for 3 hours. Afterward, the crude product was subjected to extraction with toluene, followed by three washes with water. Anhydrous magnesium sulfate was used to dry the sample, followed by filtration and concentration of the liquid phase with a rotary evaporator. The H-MQ resin was obtained as a transparent colorless viscous liquid with a 75% yield.

H-MQ ^{1}H NMR: 4.66 (s, H, SiH), 0.01 (s, CH_3).

H-MQ (20 g), EUEP (24 g), toluene (10 g), and Karstedt catalyst (2 wt% platinum, 0.025 g) were introduced into a glass flask fitted with a reflux condenser. The resulting solution was reacted at 70 °C for twelve hours. After that, toluene was removed by rotary evaporation, yielding EUEP-MQ, 43 g.

EUEP-MQ ^{1}H NMR: 6.71 (d, 1H, ArH), 6.56 (m, 2H, ArH), 4.06 (m, H, CH), 3.88 (m, H, CH), 3.72 (s, 3H, CH_3), 3.24 (s, H, CH), 2.75 (m, H, CH), 2.59 (m, H, CH), 2.43 (q, 2H, CH_2), 1.49 (t, 2H, CH_2), 0.50 (m, 2H, CH_2), 0.01 (m, CH_3).

EUEP-MQ (20 g) was transferred into a glass flask fitted with a reflux condenser. A mixture of triphenylphosphine

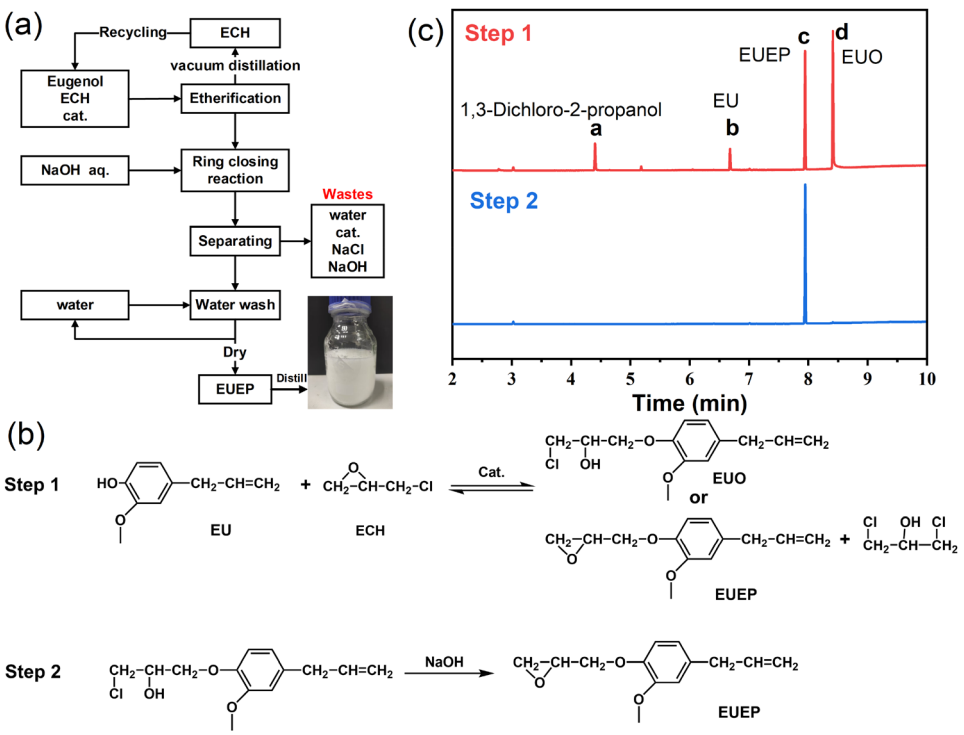

Fig. 1 (a) EUEP pilot test procedure, (b) synthesis of EUEP, and (c) GC spectra of two step products.

(0.7 g, 2.6 mmol), acrylic acid (14.4 g, 0.22 mol), and *p*-methoxyphenol (0.67 g, 5 mmol) was added into the flask dropwise over 30 minutes. The reaction mixture was agitated at 100 °C until the acid value was below 5 mg KOH per g, to obtain eugenol acrylate MQ silicone resin (EUAC-MQ), 31 g.

EUAC-MQ ^{1}H NMR: 6.73 (d, 1H, ArH), 6.54 (m, 2H, ArH), 6.29 (m, H, CH_2), 6.05 (m, H, CH_2), 5.73 (m, H, CH), 4.22 (m, H, CH_2), 4.10 (m, 2H, CH_2), 3.91 (m, 2H, CH_2), 3.67 (s, 3H, CH_3), 2.41 (m, 2H, CH_2), 1.51 (m, 2H, CH_2), 0.49 (m, 2H, CH_2), 0.01 (m, CH_3).

2.6 Preparation of the cured networks

EUAC, EUAC-MQ, $Zn(acac)_2$, and a photoinitiator were combined according to the formulation in Table 1. The blend was warmed to 80 °C until the zinc acetylacetonate completely dissolved. The resulting liquid was first cured under a 395 nm UV-LED or using a 3D printer, and then subjected to a second curing step in the oven.

3. Results and discussion

3.1 Development of a green industrial production process for EUEP

The synthesis of EUEP proceeded through two primary transformations, as shown in Fig. 1b. First, epichlorohydrin was subjected to a ring-opening etherification reaction with eugenol, producing the intermediate, eugenol chlorohydrin ether (EUO). An excess of epichlorohydrin was employed to ensure complete conversion of eugenol to EUO. In the second step, EUO was cyclized using sodium hydroxide to yield EUEP. Literature and patent sources recommended vacuum distillation after the reaction to recover excess epichlorohydrin.[32,33] However, in the second step, under alkaline conditions, the water acted as a nucleophile, attacking the chlorine atom of epichlorohydrin and generating glycerol. This side reaction reduced the purity of the recovered epichlorohydrin, limiting its potential for reuse in industrial applications.

To improve the efficiency and environmental sustainability of EUEP synthesis, we optimized the reaction protocol and characterized the products using GC-MS (Fig. 1c and Table 2); the mass spectra corresponding to each chromatographic peak are presented in Fig. S1. In the first stage, eugenol and epichlorohydrin were reacted at a 1 : 5 molar ratio. After etherification, excess epichlorohydrin was recovered *via* vacuum distillation. GC-MS analysis indicated that 92% of the eugenol was converted into EUEP (retention time: 7.9 min) and EUO (8.4 min). Notably, a portion of eugenol directly formed EUEP while simultaneously generating 1,3-dichloropropanol (4.4 min) during the initial etherification step. Due to the reversible nature of the reaction, EUO reverted to eugenol (6.7 min) upon solvent removal. Under alkaline conditions, 1,3-dichloropropanol underwent cyclization to regenerate epichlorohydrin, which subsequently reacted with residual eugenol. Meanwhile, EUO was converted to EUEP in the second step. This process yielded highly pure EUEP (98.6%) without requiring additional purification, and spontaneous crystallization at 4 °C produced white crystals.

This process significantly improves both the conversion rate and product purity (>98%), ensures high-purity epichlorohydrin recovery, and minimizes byproduct formation (only NaCl and water). Furthermore, it can be extended to other aromatic bio-based epoxy resin syntheses, such as those derived from cardanol, vanillin, and resveratrol. Compared to conventional bisphenol A glycidyl ether (BADGE)-type epoxy resin synthesis, this method offers multiple advantages, including a streamlined procedure, substantial reduction in waste emissions (gaseous, liquid, and solid), high conversion efficiency, and exceptional product purity, rendering it highly suitable for industrial-scale production.

Table 1 Formulation of photothermal curing resin

Sample	EUAC/g	EUAC-1.4MQ/g	$Zn(acac)_2$/g	Photoinitiator/g
EUAC	100	0	6	1
EUAC-MQ-10%	90	10	6	1
EUAC-MQ-20%	80	20	6	1

Table 2 Components of GC spectra

Procedure	Num.	Time/min	Component	Content/%
Step 1	A	4.4	1,3-Dichloro-2-propanol	10.6
	B	6.7	Eugenol	6.6
	C	7.9	EUEP	34.5
	D	8.4	EUO	44.3
Step 2	C	7.9	EUEP	98.6

3.2 Synthesis of EUAC and EUAC-MQ

The synthesis route for EUAC is illustrated in Fig. 2, and the ^{1}H and ^{13}C NMR spectra of EUEP and EUAC are present in Fig. 3a and b. Signals around 2.5 and 2.65 ppm, which were assigned to the epoxy ring protons of EUEP, no longer existed in the proton NMR spectrum of EUAC. Meanwhile, new peaks in the 4–4.5 ppm region appear, indicating the presence of methylene protons formed after esterification. Besides, the acrylic double bonds, exhibiting proton resonances at 6.40, 6.10, and 5.79 ppm, remain intact in the proton spectrum of EUAC. Furthermore, the ^{13}C NMR spectrum of EUAC shows the disappearance of the epoxy group signals at 49.2 and 43.9 ppm. These results confirm that the dominant transformation is esterification, excluding the possibility of acrylic double-bond polymerization.

Fig. 2 outlines the synthesis of the epoxy MQ resin, EUEP-MQ, and its esterified derivative, EUAC-MQ, with each step monitored by NMR analysis (Fig. 3c). Firstly, H-MQ was synthesized *via* the hydrolytic condensation of TEOS, followed by the capping of HMM with MM. The proton NMR spectrum revealed resonances at 4.6 and 0 ppm, which were attributed to the proton atoms in Si–H and Si–CH_3, respectively.

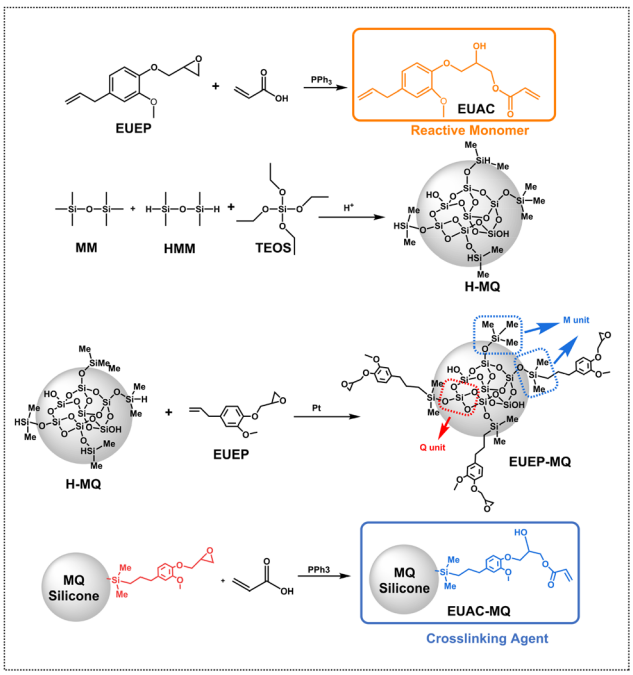

Fig. 2 Synthesis of EUAC and EUAC-MQ.

Secondly, the allyl groups of EUEP underwent hydrosilylation with H-MQ. As a result, the Si–H signal at 4.6 ppm disappeared, and new resonances appeared at 0.5 and 1.5 ppm, which were allocated to the –Si–CH_2– and –Si–CH_2–CH_2– groups, respectively. Finally, solvent was introduced to reduce system viscosity esterification and to prevent the self-polymerization of acrylic double bonds. The epoxy peaks disappeared, and –CH═CH_2 resonances were observed between 5.7 and 6.4 ppm. These data provide strong evidence for the successful synthesis of EUAC-MQ.

3.3 Curing performance of the dual photothermal bio-based resin

FT-IR spectra of EUAC, EUAC-MQ, and the resulting cured product are depicted in Fig. 3d. The absorption signal observed at 3060 cm^{-1} was assigned to the stretching vibration of ═CH_2, while the peak at approximately 1635 cm^{-1} was associated with the C═C groups. After EUAC and EUAC-MQ were mixed and cured under UV light, these peaks disappeared, indicating that the double bonds had converted to saturated bonds due to polymerization. The abundant hydroxyl groups, observed at 3500 cm^{-1}, and ester groups, observed at 1740 cm^{-1}, within the crosslinked network are likely to acceler-

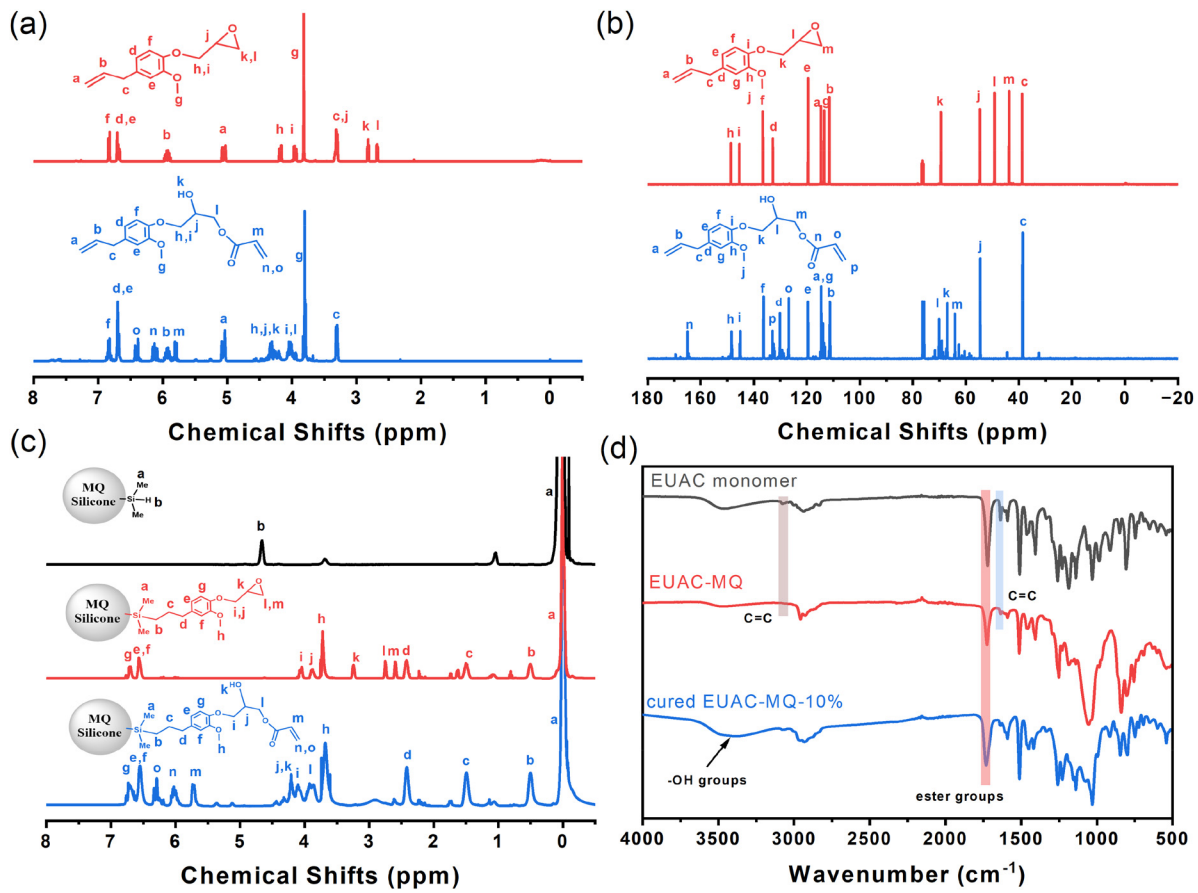

Fig. 3 NMR spectra of EUEP and EUAC: (a) ^{1}H NMR; (b) ^{13}C NMR; and (c) ^{1}H NMR spectra of EUAC-MQ; and (d) FT-IR spectra of EUAC, EUAC, and EUAC-MQ-10%.

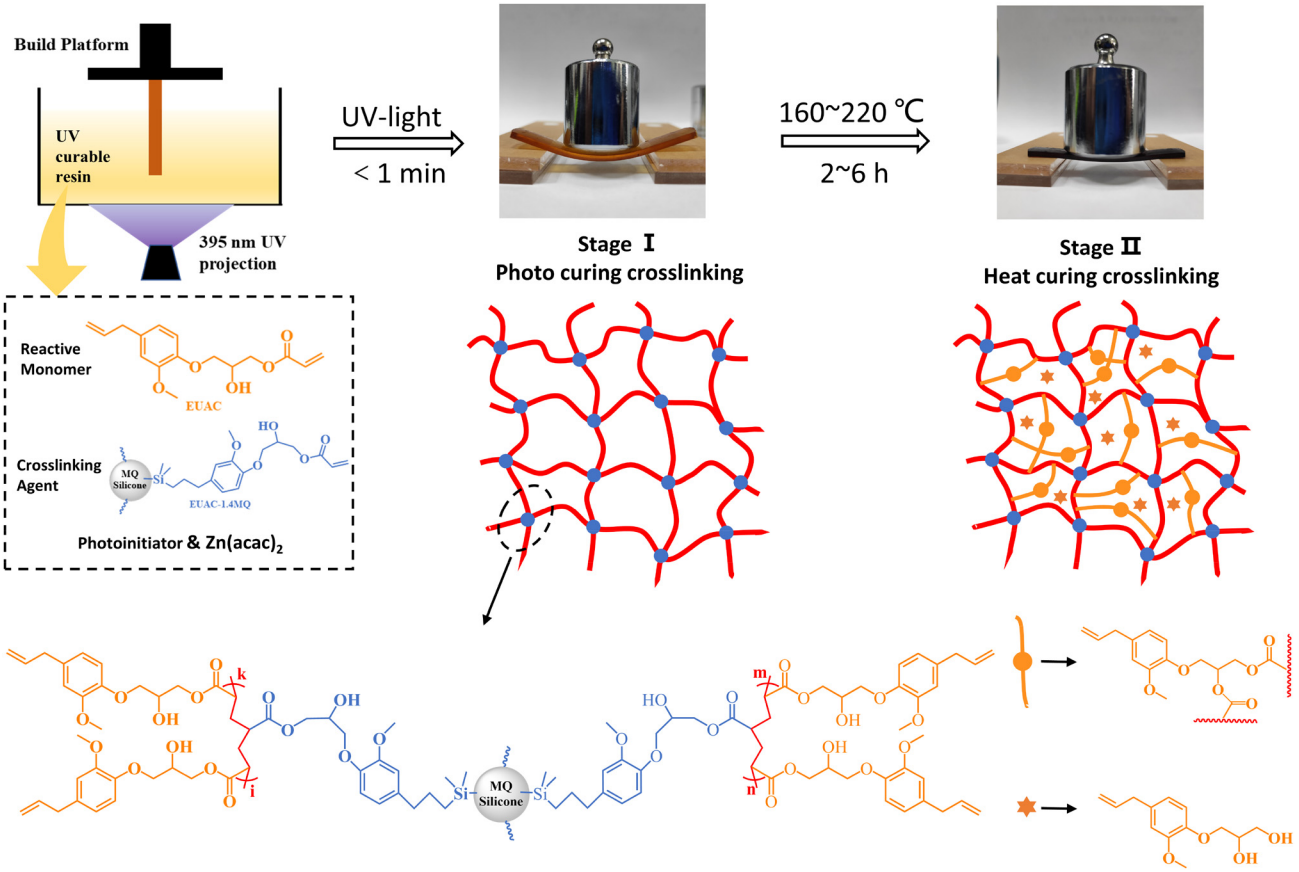

Fig. 4 Curing mechanism of photothermal curing resin.

ate the transesterification reaction during the subsequent thermosetting process.

The curing mechanism of the eugenol-based photothermal resin is shown in Fig. 4. EUAC was incorporated as the reactive monomer, with EUAC-MQ serving as the crosslinking agent in the prepolymer solution. In Stage I, the photoinitiator was activated by UV light to open the C=C bonds of both the monomer and crosslinking agent, forming permanent covalent bonds within seconds, as indicated by the red network. After photopolymerization, the cured product lacked sufficient strength, deforming under the pressure of a 200 g weight.

In Stage II, the cured resin was heated to a high temperature (180 °C), where the transesterification agent, zinc acetylacetonate, facilitated transesterification within the crosslinked network. During transesterification, ester bonds in EUAC broke and reacted with hydroxyl groups of other EUAC molecules, forming new dynamic covalent ester bonds (orange dots). Simultaneously, free diol monomers (orange stars) were generated, reacting with other ester groups. The continuous cleavage and reformation of ester bonds increased the density of crosslinking nodes while ensuring that the total covalent bond count was preserved, thereby improving the strength of the cured product. After curing and crosslinking, the specimen withstood a 200 g load without deformation.

As illustrated in Fig. S2 and Table S1, the thermal degradation performance of the cured materials with varying proportions of the crosslinking agent was investigated. The incorporation of EUAC-1.4MQ was found to enhance the thermal stability and crosslinking density of the cured materials. Specifically, the initial decomposition temperature ($T_{5\%}$) increased from 223.4 °C to a maximum of 239.3 °C with the addition of 20% EUAC-1.4MQ. The first peak degradation temperature (T_{P1}) was observed in the range of 264.2–291.3 °C, which is attributed to the degradation of free diol monomers (indicated by orange stars). Subsequently, a second degradation peak (T) occurred at approximately 390 °C for all samples, corresponding to the cleavage of C–O bonds. On the other hand, an excessive amount of MQ silicone resin led to a higher final char yield, increasing it from 26.6% to 31.9%. These thermogravimetric analysis (TGA) results demonstrate that the dual photothermal bio-based resin possesses excellent thermal stability, highlighting its potential for practical applications.

3.4 Tensile properties

Fig. 5 and Table 3 illustrate the effects of varying monomer-to-crosslinking agent ratios on the mechanical properties after different thermal treatments. Among the products cured solely by UV light, pure EUAC exhibited the lowest tensile strength, at

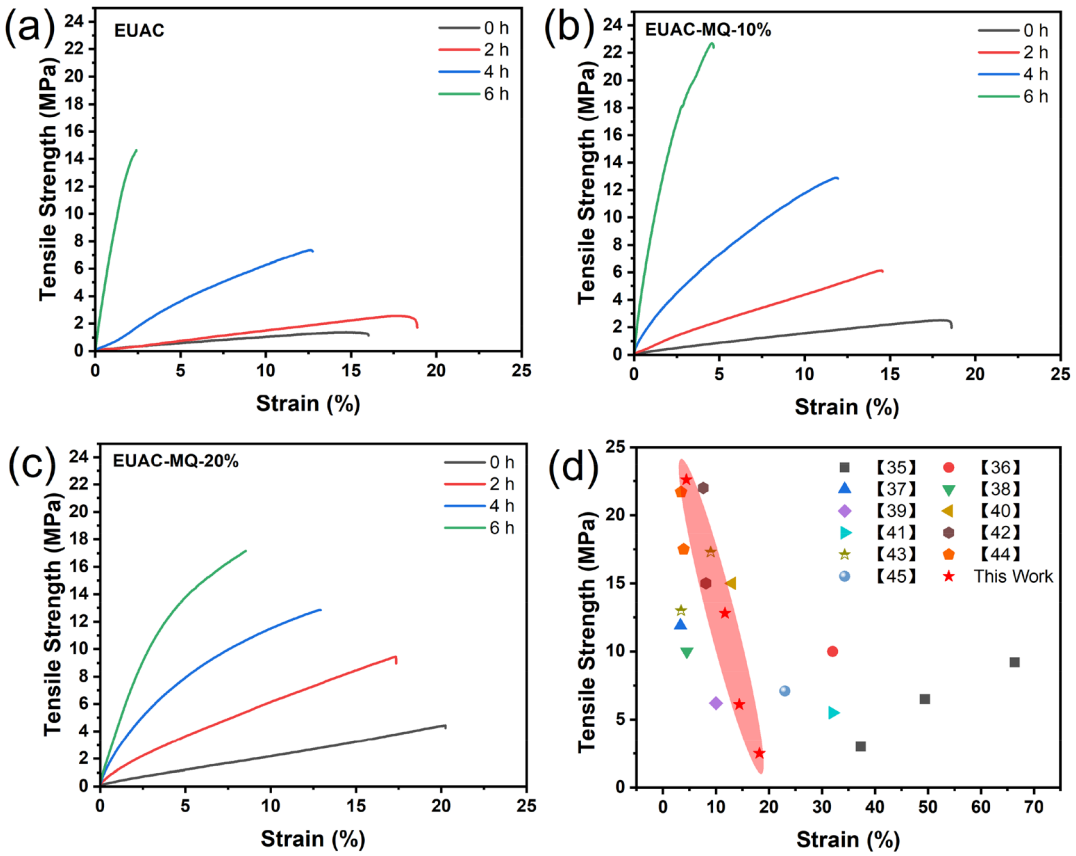

Fig. 5 Tensile curves of specimens cured at 180 °C for different times: (a) EUAC; (b) EUAC-MQ-10%; and (c) EUAC-MQ-20%; and (d) literature-reported bio-based UV-cured resin tensile properties.

only 0.5 MPa. Each EUAC monomer contained only one acrylic group, forming a linear network structure during free radical polymerization, which resulted in poor mechanical properties. Therefore, a crosslinking agent is essential for establishing a crosslinked network and enhancing mechanical strength.

Adding 10 wt% and 20 wt% EUAC-MQ increased the tensile strength of the cured material to 2.5 MPa and 4.4 MPa, respectively, while improving the elongation from 16% to 18% and 20%. Each EUAC-MQ molecule possesses more than four functional groups, which promote the creation of a crosslinked network and improve tensile strength. Additionally, prior research has highlighted that the unique cage structure of MQ silicone resin strengthens the interfacial bonds within the crosslinked network, thereby enhancing toughness.[34]

After heating the samples at 180 °C for 2, 4, and 6 hours, the tensile strength of all three specimens increased significantly with prolonged heating time. During the thermal stage, ester and hydroxyl groups underwent reversible reactions within the crosslinked network, forming new dynamic bonds in the covalent structure. It is noteworthy that during the UV curing stage, due to the absence of a crosslinking agent, the EUAC forms only a linear network. When subjected to external force, the molecular chains readily undergo relative slippage, leading to plastic deformation or failure of the material under relatively low stress. However, after heating for 2 hours, both the strength and elongation at break increase simultaneously, indicating that the network with low crosslinking density still exhibits significant mobility. Under external force, the molecular segments and the entire network can fully extend, orient, and move, thereby resulting in a large elastic deformation of 2.5 MPa and an elongation at break of 17.6%. After 6 hours of heating, the tensile strength of EUAC reached 14.6 MPa with a reduced elongation at break of 2.4%. With 10% EUAC-MQ incorporated, the tensile strength of EUAC-MQ-10% rose to 22.6 MPa, while its elongation at break improved to 4.6%. Although MQ silicone resin does not take part in transesterification, its rigid cage structure and ability to undergo plastic deformation contribute to the improved strength and toughness of the cured product. Increasing the EUAC-MQ content to 20% further raised the elongation at break to 8.6% after 6 hours of heating, but the tensile strength decreased to 17.2 MPa. Higher MQ silicone resin content could further enhance toughness, but the lower EUAC content reduced crosslinking ester exchange bonds, leading to decreased strength. Among the cured products, EUACQ-10% exhibited the best performance and will be used in subsequent testing and discussion.

As depicted in Fig. 5d, compared with literature-reported bio-based UV-cured resins including epoxidized soybean

oil,[35–39] eugenol,[40] cardanol,[41] vanillin,[42–44] and malic acid,[45] the resin developed in this work exhibits a relatively low elongation at break due to the absence of flexible segments. However, it demonstrates superior tensile strength (22.6 MPa) owing to its densely crosslinked network containing abundant rigid structures and dynamic crosslinking sites. Notably, the EUAC-MQ-10% system enables wide-range tunability of mechanical properties (tensile strength: 2.5–22.6 MPa) through simple adjustment of the heating duration, a distinctive feature not achievable in other reported resin systems. This remarkable property modulation capability provides unprecedented flexibility for tailoring material performance according to specific application requirements.

3.5 Dynamic mechanical behavior of dual photothermal bio-based resin

Fig. 6 and Table 4 present the dynamic mechanical information of EUAC-MQ-10% composites after varying thermal treatment times. The temperature of glass transition (T_g) is responsible for the main peak observed in the tan delta curves (Fig. 6a). As the thermal treatment time increased, T_g rose from 18.3 °C to 47.1 °C. Both crosslink density and backbone rigidity impact the T_g of a crosslinked polymer. New dynamic covalent bonds gradually form additional cross-linking nodes, restricting segmental movement. Simultaneously, the height of the tan δ peaks decreased from 0.65 to 0.45, indicating reduced damping and increased rigidity in the crosslinked network.

The storage modulus progression mirrored tan δ behavior, plateauing after 6 hours of treatment (Fig. 6b). This stabilization indicates equilibrium attainment in transesterification-driven network reorganization. The crosslink density (ν_c) is calculated through rubber elasticity theory using eqn (1):

$$\nu_c = E'/3RT \quad (1)$$

where E' represents the rubbery plateau modulus ($\geq T_g$ + 40 °C), R the gas constant, and T the absolute temperature. The initial crosslink density was 1268 mol m^{-3}, progressively increasing to 2000 mol m^{-3} after 4 hours as transesterification generated additional network junctions. Subsequent treatment for 6 hours maintained this density within ±1.5%, confirming dynamic bond formation saturation. This equilibrium state permitted continuous crosslink redistribution while maintaining constant network density, achieving optimal mechanical stabilization.

3.6 Stress relaxation behavior

The heat-triggered dynamic covalent bonds in the network structure rebuild the crosslinked network, promoting stress relaxation behavior. As demonstrated in Fig. 6c, the EUAC-MQ-10% system exhibited progressively accelerated relaxation rates with temperature elevation from 140 °C to 220 °C. Conventionally, the relaxation time (τ^*) was determined as the duration required for modulus decay to 1/e (36.7%) of the vitrimer's initial value. Notably, τ^* became measurable only above 160 °C, decreasing from 4904 s at 180 °C to 877 s at 220 °C. The permanent covalent network formed by photopolymerization prevented complete stress dissipation, and the sample could not fully relax even at 220 °C. Evidently, higher temperatures accelerated the dynamic exchange of covalent bonds, leading to faster relaxation. The Arrhenius equation was employed to calculate the activation energy (E_a) of the ester exchange reaction:

$$\ln\ \tau^* = \frac{E_a}{RT} - \ln A. \quad (2)$$

The stress relaxation time exhibited a strong temperature dependence, fitting well with the Arrhenius equation. As shown in Fig. 6d, an excellent linear correlation was observed. The calculated activation energy (E_a) was 68.2 kJ mol^{-1}, in agreement with previously reported values.[46]

Table 3 Mechanical properties of the cured resins

Sample	Tensile strength (MPa)	Elongation at break (%)	Young's modulus (MPa)
EUAC-0h	1.2 ± 0.2	15.6 ± 2.4	7.5 ± 0.9
EUAC-2h	2.5 ± 0.3	17.6 ± 2.1	15.0 ± 1.6
EUAC-4h	7.3 ± 0.8	12.7 ± 2.0	60.7 ± 7.5
EUAC-6h	14.6 ± 1.3	2.4 ± 0.5	1089 ± 120
EUAC-MQ-10%-0h	2.5 ± 0.3	18.2 ± 2.8	18.4 ± 2.1
EUAC-MQ-10%-2h	6.1 ± 0.7	14.4 ± 2.2	58.2 ± 6.1
EUAC-MQ-10%-4h	12.8 ± 1.2	11.7 ± 1.8	320.3 ± 35.5
EUAC-MQ-10%-6h	22.6 ± 2.5	4.4 ± 0.8	1050 ± 115
EUAC-MQ-20%-0h	4.5 ± 0.5	20.2 ± 3.1	37.3 ± 4.0
EUAC-MQ-20%-2h	9.5 ± 1.1	17.2 ± 2.5	171.5 ± 19.2
EUAC-MQ-20%-4h	12.6 ± 1.3	12.8 ± 2.1	346.2 ± 38.1
EUAC-MQ-20%-6h	17.1 ± 1.9	8.5 ± 1.4	582.9 ± 62.3

3.7 Reprocessing performance

At elevated temperatures, the dynamic ester-exchange reaction drives topological rearrangements in the network, imparting reprocessability to the material. As depicted in Fig. 7a, three polymer strips were assembled in an H-shape and heated at 200 °C for 0.5 hours without applied pressure. The crosslinked network recombined at the contact interface, resulting in a welded structure capable of supporting a 100 g weight, confirming its robust weldability. Furthermore, the crushed sample can be re-hot-pressed into a thin film at 200 °C and 10 MPa for 1 hour, demonstrating a reprocessability not found in conventional thermosetting polymers. Fig. 7b illustrates the mechanism, where hydroxyl groups initiate the cleavage of ester bonds at the interface. This process triggers dynamic ester-exchange reactions, allowing ester bonds from different interfaces to undergo exchange, thereby promoting interfacial diffusion and adhesion.[47]

This approach involved re-embedding the fractured segments. The fractured segments of the tensile specimens were re-embedded in a fresh resin matrix, which was then light-cured to form a monolithic, integrated sample. This newly formed ensemble was subsequently post-heated at 180 °C for 6 hours before tensile testing. After the fractured specimen was reassembled into a single piece, it was photocured and sub-

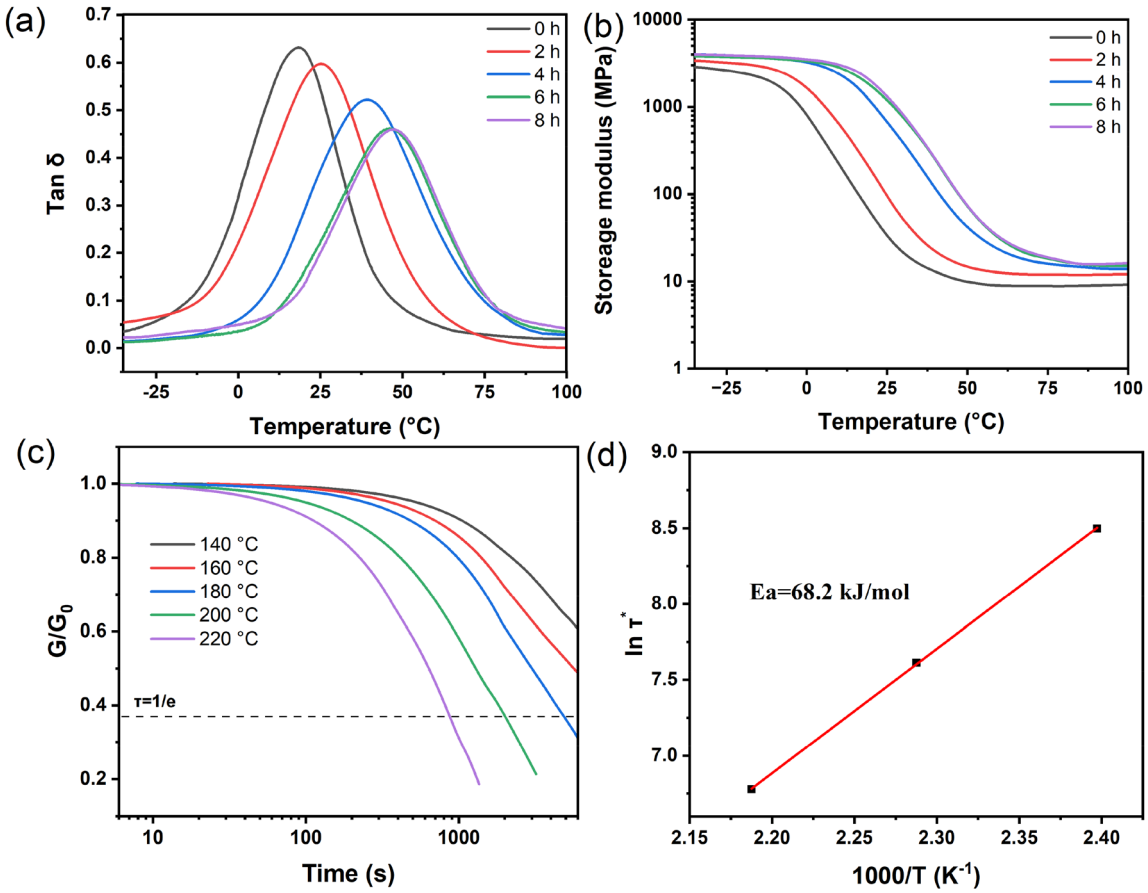

Fig. 6 DMA properties of EUAC-MQ-10% at 180 °C at different times: (a) tan δ; (b) storage modulus; normalized stress–relaxation curves (c) and Arrhenius fitting line (d) of EUAC-MQ-10% at different temperatures.

Table 4 DMA data of EUAC-MQ-10% heated in different hours

Sample	E', 25 °C (MPa)	T_g (°C)	ν_c (mol m^{-3})
EUAC-MQ-10%-0h	797.6	18.3	1268
EUAC-MQ-10%-2h	1635.3	25.5	1610
EUAC-MQ-10%-4h	3221.2	39.1	2022
EUAC-MQ-10%-6h	3339.9	46.7	2037
EUAC-MQ-10%-8h	3491.7	47.1	2049

sequently annealed at 180 °C for 6 hours. The tensile properties of the repaired material were then evaluated. As shown in Fig. 7d, the original tensile strength was 22.7 MPa, while the repaired specimen exhibited a minimal reduction in strength (21.9 MPa), with no significant change in tensile modulus. These results demonstrate that the material retains excellent mechanical integrity after repair. Furthermore, Fig. 7c reveals that fracture did not occur at the repair interface, confirming that the ester-exchange reaction restored interfacial strength to a level comparable to that of the bulk material.

3.8 3D printing

Digital light processing (DLP) technology cures materials layer by layer, offering a faster speed than fused deposition model-

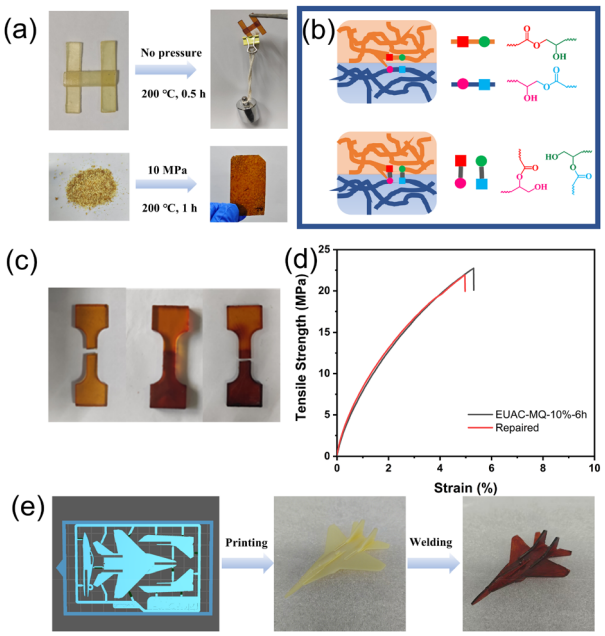

Fig. 7 Repairing and 3D printing: (a) welding and recycle test; (b) illustration of the reprocessing process; (c) photographs of the repaired samples; (d) tensile curves of the repaired samples; and (e) 2D plane model and the assembled plane model.

ing and significantly reducing printing time. This method is widely used in 3D printing. Using a photothermally curing DLP technology, we applied a eugenol-based resin to demonstrate a "print-assemble-weld" strategy. As shown in Fig. 7e, airplane model parts were rapidly printed and then assembled. Subsequent thermal curing activated dynamic ester-exchange bonds at the component interfaces, causing the parts to fuse. This process visibly eliminated the seams between the parts, resulting in a single, structurally self-supporting object. Simultaneously, dynamic transesterification increased the crosslink density, thereby enhancing its overall mechanical strength. This proof-of-concept demonstrates the material's suitability for fabricating complex structures from simpler, individually printed components that can be "welded" together post-printing.

4. Conclusion

This study pioneers a sustainable manufacturing platform for eugenol-derived vitrimers through scalable epoxidation and acrylation processes, achieving high-purity bio-based epoxy monomer synthesis (98.5%) with sustainable epichlorohydrin recovery. The engineered UV-thermal dual-curable system, integrating EUAC monomers and EUAC-MQ crosslinkers, enables dynamic network control *via* photoinitiation and transesterification synergy. Thermally activated transesterification reactions were employed to augment the crosslinking density and promote interfacial bond exchange, thereby substantially improving the material's mechanical performance and interfacial adhesion strength. The material's unique properties facilitate high-speed 3D printing through interfacial bond reformation, demonstrating superior print quality. This work establishes a commercially viable platform for manufacturing high-performance eugenol-based vitrimers with customizable mechanical properties, self-healing capacity, and recyclability, representing a significant advancement in sustainable polymer technology.

Author contributions

Jieyuan Zheng: methodology, investigation, and writing – original draft; Xingfen Huang: validation, resources, and writing – original draft; Pingwei Liu: writing – review & editing; Wenjun Wang: writing – review & editing and supervision; and Hong Fan: writing – review & editing and supervision. Jieyuan Zheng and Xingfen Huang contributed equally to this work.

Conflicts of interest

The authors declare that they have no known competing financial interests or personal relationships that could have appeared to influence the work reported in this paper.

Data availability

The data supporting this article have been included as part of the SI. See DOI: https://doi.org/10.1039/d5lp00162e.

Acknowledgements

The authors greatly appreciate the National Key R&D Programs of China (No. 2023YFD1700901), the Research Funds of Institute of Zhejiang-Quzhou (No. IZQ2023RCZX025), and Priority R&D Projects of Quzhou (No. 2024K059), and are thankful for the technical support from the State Key Lab of Chemical Engineering, Zhejiang University for the characterization of our samples.

References

1 M. Ahmadi, K. Ehrmann, T. Koch, R. Liska and J. Stampfl, *Chem. Rev.*, 2024, **124**, 3978–4020.
2 A. Bagheri and J. Jin, *ACS Appl. Polym. Mater.*, 2019, **1**, 593–611.
3 M. Sangermano, N. Razza and J. V. Crivello, *Macromol. Mater. Eng.*, 2014, **299**, 775–793.
4 Y. Lu, C. Zhang, T. Xie and J. Wu, *Chem Bio Eng.*, 2024, **1**, 76–82.
5 V. S. D. Voet, T. Strating, G. H. M. Schnelting, P. Dijkstra, M. Tietema, J. Xu, A. J. J. Woortman, K. Loos, J. Jager and R. Folkersma, *ACS Omega*, 2018, **3**, 1403–1408.
6 J. Guit, M. B. L. Tavares, J. Hul, C. Ye, K. Loos, J. Jager, R. Folkersma and V. S. D. Voet, *ACS Appl. Polym. Mater.*, 2020, **2**, 949–957.
7 T. O. Machado, C. J. Stubbs, V. Chiaradia, M. A. Alraddadi, A. Brandolese, J. C. Worch and A. P. Dove, *Nature*, 2024, **629**, 1069–1074.
8 X. Feng and G. Li, *ACS Appl. Mater. Interfaces*, 2020, **12**, 57486–57496.
9 Y. Nie, R. Liu, N. Yao, T. Deng, R. Yan, S. Li, M. Li, X. Yang, H. Ding and L. Xu, *Polym. Test.*, 2023, **118**, 107879.
10 M. Das, A. R. Parathodika, P. Maji and K. Naskar, *Eur. Polym. J.*, 2023, **186**, 111844.
11 S. Ji, W. Cao, Y. Yu and H. Xu, *Angew. Chem., Int. Ed.*, 2014, **53**, 6781–6785.
12 M. Xie, L. Wang, F. Liu, D. Zhang and J. Gao, *J. Phys. Chem. A*, 2016, **120**, 9081–9088.
13 S. Grauzeliene, A.-S. Schuller, C. Delaite and J. Ostrauskaite, *Eur. Polym. J.*, 2023, **198**, 112424.
14 Y.-Y. Liu, G.-L. Liu, Y.-D. Li, Y. Weng and J.-B. Zeng, *ACS Sustainable Chem. Eng.*, 2021, **9**, 4638–4647.
15 J. Aizpurua, L. Martin, M. Fernández, A. González and L. Irusta, *Prog. Org. Coat.*, 2020, **139**, 105460.
16 M. Bin Rusayyis and J. M. Torkelson, *Macromolecules*, 2020, **53**, 8367–8373.

17 A. Zych, J. Tellers, L. Bertolacci, L. Ceseracciu, L. Marini, G. Mancini and A. Athanassiou, *ACS Appl. Polym. Mater.*, 2020, **3**, 1135–1144.
18 D. Montarnal, M. Capelot, F. Tournilhac and L. Leibler, *Science*, 2011, **334**, 965–968.
19 M. Capelot, M. M. Unterlass, F. Tournilhac and L. Leibler, *ACS Macro Lett.*, 2012, **1**, 789–792.
20 A. Demongeot, S. J. Mougnier, S. Okada, C. Soulié-Ziakovic and F. Tournilhac, *Polym. Chem.*, 2016, **7**, 4486–4493.
21 B. Zhang, K. Kowsari, A. Serjouei, M. L. Dunn and Q. Ge, *Nat. Commun.*, 2018, **9**, 1831.
22 G. Arias-Ferreiro, A. Ares-Pernas, A. Lasagabáster-Latorre, M. S. Dopico-García, P. Ligero, N. Pereira, P. Costa, S. Lanceros-Mendez and M. J. Abad, *Adv. Mater. Technol.*, 2022, **7**, 2101503.
23 A. Navaruckiene, D. Bridziuviene, V. Raudoniene, E. Rainosalo and J. Ostrauskaite, *Materials*, 2021, **14**, 653.
24 P. Bednarczyk, A. Wróblewska, A. Markowska-Szczupak, P. Ossowicz-Rupniewska, M. Nowak, M. Kujbida, A. Kamińska and Z. Czech, *Coatings*, 2021, **11**, 1556.
25 H. Bhanushali, S. Mestry and S. T. Mhaske, *J. Appl. Polym. Sci.*, 2023, **140**, 53817.
26 J. Wu, Y. Qian, C. A. Sutton, J. J. La Scala, D. C. Webster and M. P. Sibi, *ACS Sustainable Chem. Eng.*, 2021, **9**, 15537–15544.
27 M. Derradji, O. Mehelli, W. Liu and N. Fantuzzi, *Front. Chem.*, 2021, **9**, 691117.
28 H. Qiang, J. Wang, H. Liu and Y. Zhu, *Polym. Chem.*, 2023, **14**, 4255–4274.
29 B. Y. Karlinskii and V. P. Ananikov, *Chem. Soc. Rev.*, 2023, **52**, 836–862.
30 C. Li, H. Fan, T. Aziz, C. Bittencourt, L. Wu, D.-Y. Wang and P. Dubois, *ACS Sustainable Chem. Eng.*, 2018, **6**, 8856–8867.
31 J. Zheng, Y. Cai, X. Zhang, J. Wan and H. Fan, *ACS Appl. Polym. Mater.*, 2022, **4**, 929–938.
32 Â. Lima, W. de Paula, I. Leite, P. Gazolla, L. de Abreu, V. Fonseca, W. Romão, V. Lacerda Jr, V. de Queiroz, R. Teixeira and A. Costa, *J. Braz. Chem. Soc.*, 2022, **33**, 1200–1210.
33 C. Aouf, C. Le Guernevé, S. Caillol and H. Fulcrand, *Tetrahedron*, 2013, **69**, 1345–1353.
34 J. Zheng, Y. Cai, Y. Hu, J. Zhu, J. Wei, Y. Ma, J. Wan and H. Fan, *Polym. Chem.*, 2022, **13**, 5325–5336.
35 M. Fei, T. Liu, B. Zhao, A. Otero, Y.-C. Chang and J. Zhang, *ACS Appl. Polym. Mater.*, 2021, **3**, 2470–2479.
36 J. Peng, C. Zhou, B. Chen, H. Zhang, X. Pan, W. Xiong, X. Luo and Y. Liu, *Ind. Crops Prod.*, 2024, **209**, 117958.
37 Y. Zhou, L. Feng and J. Qu, *J. Coat. Technol. Res.*, 2023, **20**, 1923–1933.
38 R. P. Rosa, G. Rosace, R. Arrigo and G. Malucelli, *J. Polym. Res.*, 2023, **30**, 139.
39 D. Lascano, J. Gomez-Caturla, D. Garcia-Sanoguera, D. Garcia-Garcia and J. Ivorra-Martinez, *Mater. Des.*, 2024, **243**, 113084.
40 K. Lian, S. Yang, D. Lu, W. Tang and J. Zhang, *ACS Appl. Polym. Mater.*, 2024, **7**, 445–456.
41 R. Liu, X. Zhang, J. Zhu, X. Liu, Z. Wang and J. Yan, *ACS Sustainable Chem. Eng.*, 2015, **3**, 1313–1320.
42 Y. Xu, K. Odelius and M. Hakkarainen, *ACS Sustainable Chem. Eng.*, 2020, **8**, 17272–17279.
43 A. Liguori, S. Subramaniyan, J. G. Yao and M. Hakkarainen, *Eur. Polym. J.*, 2022, **178**, 111489.
44 G. Motiekaityte, A. Navaruckiene, V. Raudoniene, D. Bridziuviene, J. Jaras, K. Kantminiene and J. Ostrauskaite, *J. Appl. Polym. Sci.*, 2022, **140**, e53289.
45 J. Zhang, J. Huang, G. Zhu, X. Yu, J. Cheng, Z. Liu, Y. Hu, Q. Shang, C. Liu, L. Hu and Y. Zhou, *Green Chem.*, 2021, **23**, 5875–5886.
46 K. Yu, P. Taynton, W. Zhang, M. L. Dunn and H. J. Qi, *RSC Adv.*, 2014, **4**, 48682–48690.
47 J. Wu, X. Yu, H. Zhang, J. Guo, J. Hu and M.-H. Li, *ACS Sustainable Chem. Eng.*, 2020, **8**, 6479–6487.